A Physics-Aware MIQP Approach to Harmonic State Estimation in Low-Observable Power Distribution Systems Using Harmonic Phasor Measurement Units

Fatemeh Ahmadi-Gorjayi, *Student Member, IEEE*, Hamed Mohsenian-Rad, *Fellow, IEEE*

***Abstract*—In this paper, a novel *physics-aware* harmonic state estimation (HSE) method is developed for power distribution systems with low-observability. The only available measurements are the *harmonic synchrophasors* from a small number of Harmonic Phasor Measurement Units (H-PMUs) on a power distribution feeder. The proposed HSE method provides a novel and practical application of H-PMUs, which are an emerging class of *smart grid sensors*, in order to address an important and challenging problem in power distribution system monitoring. More importantly, the proposed HSE method can address the highly challenging scenario, in which, not only the network has a low-observability condition, but also the number and the location(s) of the harmonic sources are *unknown*. The proposed HSE method captures *physics-based sparsity pattern* in the analysis of harmonic phasors, and then it incorporates such sparsity pattern in the formulation of a novel *mixed-integer quadratic programming* (MIQP) optimization which can be solved by standard solvers. The method that is proposed in this paper to address low-observability is innovative and it is *specific* to HSE. It does *not* have any similar counterpart in the literature, whether for harmonic state estimation for in ordinary (i.e., not harmonic) distribution system state estimation. The effectiveness of the proposed method is tested and confirmed in multiple case studies and compared with the existing methods.**

***Keywords*–Harmonic phasor measurement units, harmonic state estimation, physics-aware method, power distribution networks, radial topology, low-observability.**

I. Introduction

A. Motivations

Situational awareness about harmonic distortions is a critical task in power systems monitoring in power distribution systems. The importance of this task has further increased in recent years due to the increasing number of power electronic devices, nonlinear loads, and inverter-based energy resources; all of which can potentially add to harmonic distortions. Harmonic pollution can cause failures in reliable and secure operation of power distribution systems by overheating the conductors or interfering with the power protection systems [1]. Therefore, utilities are required to monitor and limit harmonic levels in power distribution systems [2].

Harmonic State Estimation (HSE) is the key to build a real-time monitoring system to assist the power distribution system operator to pinpoint the harmonic sources; and accordingly, to provide information about the propagation of the harmonics in voltage and current across the power distribution feeder.

The authors are with Department of Electrical and Computer Engineering, University of California, Riverside, CA, USA. E-mails: fahma012@ucr.edu and hamed@ece.edu. This work was supported by the National Science Foundation grant 1711944. The corresponding author is H. Mohsenian-Rad.

However, a major challenge in this field is the limited deployment of power quality sensors at the distribution level in real-world power systems. This area has recently received a boost with the development of *Harmonic Phasor Measurement Units* (H-PMUs), which are an emerging class of smart grid sensors. H-PMUs provide time-synchronized harmonic voltage and current phasor measurements, see [3]–[8] for more details. However, it is still cost-prohibitive and impractical to place such advanced sensors at every bus to reach full-observability.

This raises the question on how we can achieve situational awareness on harmonic phasors and power quality in power distribution systems, while using only a few H-PMUs.

B. Related Work

While there is a rich literature on the study of HSE at the transmission level [9]–[14], the literature on the study of the HSE at the distribution level is still limited [15]–[20]. This is because, HSE is a relatively new problem at power distribution systems in practice. It has been emerging as a viable effort only recently due to the recent advancements in instrumentation and sensor deployments at power distribution systems.

However, there are major differences between conducting HSE at the transmission level and conducting it at the distribution level. There are at least two reasons for these differences. The first issue is the lack of measurement redundancy at distribution level; even lack of sufficient measurements to achieve basic observability. Importantly, most of the existing HSE methods are meant to be used at transmission level with sufficient harmonic phasor measurements such that the network is *fully-observable* [21]. The second issue is the nature of all radial topologies in power distribution networks. Inherently, there is *less coupling* among the harmonic voltage phasors across different buses in a radial network topology; because each bus has at most only two immediate neighboring buses. This is very different from the tight coupling among the harmonic voltage phasors in a meshed network topology, which is common in power transmission systems. Therefore, one cannot simply reuse the HSE methods that are developed for the transmission level at the distribution level. For a power distribution system that has a radial topology, numerous harmonic measurement devices (and their associated communication infrastructures) are needed in order to make the system fully-observable; but this is cost prohibitive.

Therefore, the ability to work under the *low-observability* conditions is a necessary feature for an effective HSE method that is meant to be used in power distribution networks.

Accordingly, we can divide the existing literature on HSE at power distribution systems into two groups. First, the HSE

methods that do *not* explicitly address low-observability, e.g., in [16], [17]. Second, the HSE methods that *do* explicitly mention the need to address low-observability [15], [18]–[20].

The methods in the first group usually fail to provide accurate results when the network is *not* observable. This is because they are *not* designed to work under such circumstances.

As for the methods in the second group, that do recognize the need to address low-observability in the HSE problem at distribution level, a common approach is to use pseudo-measurements (such as historical data) to make the network fully-observable, e.g., see [16], [22]. However, uncertainty and error in historical data have huge impact on the accuracy of the HSE methods that need to rely on pseudo-measurements.

Another approach to tackle low-observability in the HSE problem is to use mathematical techniques to deal with the rank deficiency of equations in the HSE problem. In [15], [19], HSE methods are proposed based on singular value decomposition to formulate the HSE problem at distribution level as a least square optimization and to solve it by obtaining the pseudo-inverse of the low-rank measurement matrix. In [18], an HSE method is proposed based on sparse Bayesian learning which involves using regression for power flow analysis and recurrent neural network models for demand prediction.

In [13], the HSE problem is formulated as a constrained sparsity maximization which is solved by linear programming. Although this work was tested on the 14-bus power transmission system, since the methodology does not depend on the inherent properties of the transmission level, it has the basic capabilities to be applied to power distribution systems as well. Compressed sensing is used also in [23], where the focus is on the case with only one harmonic source in the network.

Although sparse recovery is generally considered effective in finding the sparse solution for an undetermined system of equations, the mathematical conditions that may guarantee its performance are usually very specific and do not hold in the HSE problem, specially if there is *more than one* harmonic source of the same harmonic order in the system [23].

There are also methods that are *not* meant to solve the HSE problem; but they seek to estimate and identify the location of the harmonic source(s) at the distribution level [21], [24]–[26]. These methods are very different from HSE; because they do *not* estimate the harmonic state variables across the power distribution network. In [24], a Bayesian approach is proposed to locate the harmonic source. In this method, the information to indicate the possible presence of the harmonic source as well as a metric about the reliability of such metric are discussed. In [25], a method is proposed based on particle swarm optimization to locate and estimate the parameters of the harmonic source with the highest contribution. In [21], a method based on exhaustive search is developed to locate and estimate multiple sources of harmonics in a low-observable power distribution system. Importantly, the methods in [21], [24]–[26] are *not* designed to solve the HSE problem.

Another subject that is widely discussed in the literature is the task of sensor placement in power systems, including the placement of harmonic sensors. Different methods have been used, such as integer programming [27], quadratic programming [28], genetic algorithm [29] and neural networks [30]. However, sensor placement is beyond the scope of this paper.

Last but not least, it is worth emphasizing that, when it comes to the HSE problem, the issue with low-observability is with respect to the *harmonics* in the system. It is *not* with respect to the *fundamental* component. It is possible that a power distribution system *is* observable at the fundamental frequency, but it is *not* observable at the harmonics. Note that, observability at the fundamental frequency can be achieved or reinforced by using different types of sensors, including PMUs and smart meters, which are widely deployed by many utilities. Therefore, there can be several sensors available for an ordinary state estimation at the fundamental frequency. The literature on addressing low-observability in ordinary (i.e., not harmonic) distribution system state estimation is separate, such as in [31]–[34]. However, in practice, we have a few harmonic sensors available for harmonic state estimation. Consequently, it might be possible for a power system to be observable at the fundamental frequency, but not at certain harmonics.

C. Summary of Contributions

The method that is proposed in this paper to address low-observability is innovative and it is *specific* to HSE and completely new. It does *not* have any similar counterpart in the literature, whether in harmonic state estimation or in ordinary (i.e., not harmonic) distribution system state estimation. The main contributions in this paper are summarized as follows:

1) A new *physics-aware* HSE method is developed for power distribution systems with low-observability due to the availability of only a few H-PMUs. The "physics-awareness" is due to extracting physics-based sparsity patterns of harmonic nodal voltage phasors, harmonic nodal injection current phasors, and harmonic line current phasors in the presence of harmonic sources.
2) Importantly, the proposed method can tackle the challenges when there are multiple harmonic sources of the same harmonic order on the power distribution feeder, while the *number* and *locations* of the harmonic sources are *unknown*. This is a major achievement; specially due to the low-observability of the power distribution system.
3) The proposed HSE method integrates the captured physics-aware sparsity characteristics into the formulation of a novel mixed-integer quadratic programming (MIQP) formulation, instead of taking the approach of a typical sparse recovery optimization. The advantages of such alternative approach are discussed and verified.

Various case studies are conducted to examine the performance of the proposed HSE method in addressing low-observability in comparison with selected comparable methods in the literature. The case studies also address sensitivity analysis, with respect to the number and the location(s) of the harmonic sources as well as the numbers and location(s) of H-PMUs, and the number of harmonic orders.

II. System Model

Let $G := (N; L)$ denote the graph representation of a radial power distribution feeder, where N is the set of all buses and L

is the set of all line segments. An example is shown in Fig. 1, where the network topology is based on the IEEE 33-bus test system. For each harmonic order h in the system, we assume that $\mathbf{I}_N(h)$ denotes the vector of the harmonic nodal current injection phasors at all the buses in set N. Similarly, let $\mathbf{I}_L(h)$ denote the vector of the harmonic line current phasors at all the line segments in set L; and let $\mathbf{V}(h)$ denote the vector of the harmonic nodal voltage phasors at all the buses in set N.

A. Basic HSE Problem Formulation

At each harmonic order h, we define the vector of the harmonic state variables in the power system as follows:

$$\mathbf{X}(h) = [(\mathbf{I}_N(h))^{>}(\mathbf{I}_L(h))^{>}(\mathbf{V}(h))^{>}]^{>}; \tag{1}$$

Our goal is to estimate the above vector of state variables by using harmonic synchrophasor measurements from H-PMUs. Each H-PMU measures the harmonic nodal voltage phasors and the harmonic line current phasors at its location.

Let $\mathbf{Z}(h)$ denote the vector of all available harmonic synchrophasor measurements that are collected from the H-PMUs:

$$\mathbf{Z}(h) = [(\mathbf{V}^m(h))^{>}(\mathbf{I}_L^m(h))^{>}]^{>}; \tag{2}$$

where superscript m indicates the measurements to distinguish them from the state variables. Also, let us define $\mathbf{H}(h)$ as the harmonic measurement matrix, which captures all the mappings between the harmonic synchrophasor measurements in $\mathbf{Z}(h)$ and the harmonic state variables in $\mathbf{X}(h)$ as:

$$\mathbf{Z}(h) = \mathbf{H}(h)\,\mathbf{X}(h) + \mathbf{e}(h); \tag{3}$$

where $\mathbf{e}(h)$ is the corresponding vector for measurement noise. The construction of matrix $\mathbf{H}(h)$ is discussed in Appendix A.

The HSE problem is then formulated as follows:

$$\underset{\mathbf{x}(h)}{\textbf{minimize}} \quad \|\mathbf{Z}(h) - \mathbf{H}(h)\mathbf{X}(h)\|_2^2; \tag{4}$$

If matrix $\mathbf{H}(h)$ is full-ranked, then the network is fully-observable at harmonic order h and the least-square problem in (4) has a unique solution. This happens only if we install a large number of H-PMUs across the distribution circuit.

B. Augmented HSE Problem Formulation

A power system is said to be *fully-observable* in the domain of harmonics, if the harmonic state variables at all buses and/or all line segments can be uniquely obtained from the available harmonic phasor measurements. An analytical interpretation of full-observability is that the measurement matrix $\mathbf{H}(h)$ must be full-rank. To achieve full-observability in a radial power distribution feeder, the grid operator must install H-PMUs at least at half of the buses. However, this is *not* a realistic option, because of the high cost of H-PMUs, including the cost of sensors, the cost of sensor installation, and the cost of setting up a communication infrastructure for data collection. As a result, power distribution systems are often inherently subject to low-observability, specially when it comes to solving the HSE problem. For instance, for the case of the network in Fig. 1, we may face a scenario where only five H-PMUs are available; one at the substation; one at the end of the main; and three at the end of each of the three laterals.

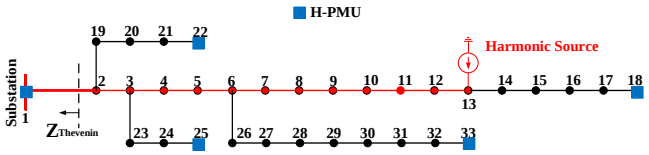

Fig. 1. An example distribution feeder with one harmonic source. In practice, the harmonic current almost entirely flows through the substation.

Therefore, in practice, the network is *not* fully-observable; and it is a challenge to solve the HSE problem in (4).

To properly address this challenge, we focus on an *augmented* version of the HSE problem as follows:

$$\underset{\mathbf{x}(h)}{\textbf{minimize}} \quad \left\| \begin{bmatrix} \mathbf{Z}(h) \\ \mathbf{0} \end{bmatrix} - \begin{bmatrix} \mathbf{H}(h) \\ \mathbf{G}(h) \end{bmatrix} \mathbf{X}(h) \right\|_2^2; \tag{5}$$

where $\mathbf{G}(h)$ is a matrix that captures the relationships among the harmonic state variables, in particular between $\mathbf{V}(h)$ and $\mathbf{I}_L(h)$, by using the circuit equations. More details about the construction of matrix $\mathbf{G}(h)$ is provided in Appendix A.

For a network that *is* fully-observable, there is no advantage to use the augmented HSE formulation in (5) compared to the basic HSE formulation in (4). However, when the network is *not* fully-observable, it is necessary to use the augmented formulation to at least include the unobservable variables in the equations of the HSE problem formulation; otherwise they cannot be even part of the analysis; because they would not show up in any equation. Thus, for the rest of this paper, we focus on the augmented HSE problem formulation in (5).

Next, we consider three different scenarios: a) the case where there is one harmonic source in the network; b) the case where the are multiple harmonic sources in the network; and c) the case where the number of harmonic sources is unknown.

III. Physics-Aware HSE Solution: One Harmonic Source

In this section, we discuss a scenario where there is exactly one harmonic source in the network. The immediate result of this assumption is that exactly one entry in vector $\mathbf{I}_N(h)$ is non-zero; while all the other entries are zero. In other words, there is an inherent *sparsity* in the construction of vector $\mathbf{I}_N(h)$, which can be mathematically expressed as:

$$\mathbf{e}_i^{>}\,\mathbf{I}_N(h) = 0; \quad 8\, i \,2\, N n f k g; \tag{6}$$

where k is the bus number for the location of the harmonic source; and $\mathbf{e}_i$ is a standard basis vector with all its entries being equal to zero, except for the entry at row i which is one.

Given the radial topology of the power distribution systems, one may ask: how does the inherent sparsity in vector $\mathbf{I}_N(h)$ may create sparsity in vectors $\mathbf{I}_L(h)$ and $\mathbf{V}(h)$?

Next, we answer this question by using the physical characteristics of the underlying power distribution circuit. Accordingly, we build the foundation for our proposed physics-aware HSE solution for low-observable power distribution systems.

A. Fundamental Sparsity in Radial Networks

Again Consider the power distribution feeder in Fig. 1. Suppose there is exactly one harmonic source in the network. Suppose the harmonic source is at bus 13. The harmonic source injects the harmonic current to the distribution feeder; accordingly, it is modeled as a current source in Fig. 1.

As it is shown in [8], [35], [36], and also explained in Appendix B, the injected harmonic current at bus 13 almost entirely flows through the substation and *not* through the loads. The reason is that the impedance in the Thevenin equivalent of the substation that is seen by the distribution feeder, which is marked by Z_{Thevenin} in Fig. 1, is much less than the impedance of the loads on the distribution feeder. Thus, almost the entire harmonic current that is injected by the harmonic source passes through the *substation connector* path, i.e., the lines that are marked in red, from bus 13 all the way up to the substation.

We can analyze the impact of injecting harmonic current by a harmonic source at any other bus in the network in a similar way, i.e., based on the substation connector path between the location of the harmonic source and the substation.

From the above physics-based observation in radial networks, together with the inherent sparsity in (6), we can conclude that the entries in vector $\mathbf{I}_L(h)$ that are associated with the line segments on the connector path between bus k and the substation are non-zero; while all the other entries are almost zero. In other words, the entries in $\mathbf{I}_L(h)$ that correspond to the line segments in set L_k are non-zero; while the entries in $\mathbf{I}_L(h)$ that correspond to the line segments in set $L \setminus L_k$ are zero. This can be mathematically expressed as:

$$\mathbf{e}_l^{\top}\, \mathbf{I}_L(h) \quad 0; \quad 8\, l \in L \setminus L_k; \tag{7}$$

where L_k is the set of all line segments that belong to the substation connector path for bus k. Note that, $L_k \quad L$.

The zero approximations in harmonic currents in (6) and (7) also have implications on nodal harmonic voltages in $\mathbf{V}(h)$. To see this, let us define N_k as the set of all buses that are on the substation connector path for bus k. Furthermore, for each bus i in set $N \setminus N_k$, let us define $p(k;i)$ as the bus that is the most downstream *parent* of bus i that belongs to set N_k. For example, for the scenario in Fig. 1 with $k = 13$, we have:

$$p(13;23) = p(13;24) = p(13;25) = 3. \tag{8}$$

This is because bus 3 is the most downstream parent of buses 23, 24, and 25 that belongs to the substation connector path between bus 13 and the substation. From (7), the harmonic voltage phasor at buses 23, 24, and 25 is almost equal to the harmonic voltage phasor at bus 3. This comes from the fact that there is no harmonic current on the line between buses 3 and 23, the line between buses 23 and 24, and the line between buses 24 and 25; therefore, there is no harmonic voltage difference across buses 3, 23, 24, and 25. This leads to the following voltage approximation in the power system:

$$\mathbf{e}_i^{\top}\, \mathbf{V}(h) \quad \mathbf{e}_{p(k;i)}^{\top} \mathbf{V}(h) \quad 0; \quad 8\, i \in N \setminus N_k. \tag{9}$$

As a result, we do *not* need to estimate all the harmonic voltage phasors in the system. Instead, we can only estimate harmonic voltage phasors at the buses that are on the substation connector path for bus k. The rest of the harmonic voltage phasors are then readily obtained from the approximation in (9).

Summary: Based on the analysis in (6), (7), and (9), the total number of harmonic state variables that we need to estimate for the scenario with one harmonic source at bus k is:

$$|N_k| + |L_k| + 1. \tag{10}$$

In other words, since the total number of harmonic state variables of harmonic order h in the system is $2|N| + |L|$, the total number of harmonic state variables that we can readily obtain from the results in (6), (7), and (9) is:

$$2|N| + |L| \quad |N_k| \quad |L_k| \quad 1. \tag{11}$$

For example, for the scenario in Fig. 1, the number of state variables to estimate is $13 + 12 + 1 = 26$. The remaining 72 variables are readily obtained from (6), (7), and (9).

B. Physics-Aware MIQP Formulation

In this section, we integrate the physics-based approximations in (6), (7), and (9) into the formulation of the augmented HSE problem in (5). This is done by introducing a novel and tractable mixed-integer formulation for the HSE problem.

Let us define b as an $|N| \quad 1$ vector of binary variables. For each row k, the corresponding entry is 1 if the harmonic source is located at bus k; otherwise the entry is 0. From (6), we know that exactly one entry in b is 1 and all other entries are 0. This can be mathematically expressed as:

$$\mathbf{1}^{\top} b = 1. \tag{12}$$

Also, from (6), we know that harmonic nodal injection current is zero for all the buses in $N \setminus \{k\}$. We can express this sparsity pattern through the defined binary variables as:

$$M\, b \quad \mathbf{I}_N(h) \quad M\, b; \tag{13}$$

where M is a large number. In total, there are $|N|$ rows of both lower-bound and upper-bound inequalities in (13). From (13), together with (12), the harmonic nodal injection current is zero for all the buses in $N \setminus \{k\}$, i.e., all the buses that are *not* the location of the harmonic source. For any of such buses, the corresponding row in (13) forms a pair of a *lower bound at zero* and an *upper bound at zero*; thus, forcing the harmonic current injection to be zero. This is done *without* knowing the location of the harmonic source in advance; because the constraints in (13) are defined based on the binary vector b.

It is worth mentioning that, the constraints in (13) have no impact on the harmonic nodal injection current at the location of the harmonic source. This is because the corresponding lower bound and the corresponding upper bound would be ineffective; due to the fact that M is a large number.

In order to incorporate the binary vector b in the approximate equality constraints in (7) and (9), let us first define:

$$U = \sum_{k \in N} |L \setminus L_k|; \quad W = \sum_{k \in N} |N \setminus N_k|: \tag{14}$$

Here, U denotes the total number of the zero approximations in the form in (7) for *all possible choices* for the location of

the harmonic source. Similarly, W denotes the total number of the zero approximations in the form in (9) for *all possible choices* for the location of the harmonic source. Depending on the location of the harmonic source, i.e., depending on which exact entry in vector b is 1, some of these zero approximations must be used and some of them must be disregarded.

Accordingly, we can express the zero approximations in (7) based on the defined binary variables as follows:

$$M \quad (1 \quad b) \quad \mathsf{A}\, \mathsf{I}_L(h) \quad M \quad (1 \quad b); \qquad (15)$$

where is a matrix of size $U \quad jNj$; and A is a matrix of size $U \quad jLj$. In each row of matrix , exactly one entry is 1, and all the other entries are zero. Similarly, in each row of matrix A, exactly one entry is 1, and all the other entries are zero. In total, there are U rows of both lower-bound and upper-bound inequalities in (15). From (15), together with (12), the harmonic line current is zero for all the lines in set LnL_k, i.e., for all the lines that are *not* on the connector path between the location of the harmonic source and the substation. For all such lines, the corresponding rows in (15) form a pair of a *lower bound at zero* and an *upper bound at zero*; thus, forcing them to be zero. This is achieved *without* knowing the location of the harmonic source in advance; because the constraints in (15) are directly defined based on the binary vector b.

Finally, we can also express the zero approximations in (9) based on the defined binary variables as follows:

$$M \quad (1 \quad b) \quad \mathsf{B}\, \mathsf{V}(h) \quad M \quad (1 \quad b); \qquad (16)$$

where is a matrix of size $W \quad jNj$; and B is also a matrix of size $W \quad jNj$. In each row of matrix , exactly one entry is 1, and all the other entries are zero. In each row of matrix B, exactly one entry is 1, exactly one entry is 1, and all the other entries are zero. In total, there are W rows of both lower-bound and upper-bound inequalities in (16). From (16), together with (12), the equality in (9) holds for any bus in set NnN_k for any choice of bus k as the location of the harmonic source. Just like in (13) and (15), this is achieved *without* knowing the location of the harmonic source in advance; because the constraints in (16) are defined based on the binary vector b.

We are now ready to reformulate the HSE optimization problem as follows, where the physics-aware sparsity patterns are fully integrated into the problem formulation:

$$\underset{\mathsf{x}(h);b}{\textbf{minimize}} \quad \begin{matrix} \mathsf{Z}(h) \\ 0 \end{matrix} \quad \begin{matrix} \mathsf{H}(h) \\ \mathsf{G}(h) \end{matrix} \quad \mathsf{X}(h) \quad \begin{matrix} 2 \\ \\ 2 \end{matrix} \qquad (17)$$

subject to Eqs. (1); (12); (13); (15); (16):

The above optimization problem is an MIQP, where the objective function is a standard Least-Square (LS) formulation over *continuous* variables, while the constraints are linear mixed-integer. The MIQP in (17) can be solved by using various optimization solvers, including CVX toolbox in MATLAB [37]. Once the optimal solutions are obtained, the only non-zero entry in b pinpoints the host bus for the harmonic source; and $\mathsf{X}(h)$ provides us with the estimation of harmonic state variables. Therefore, the proposed HSE method not only does not need any prior information about the location of harmonic source, but also it gives us the exact host location in addition to the estimation results under the low-observability conditions.

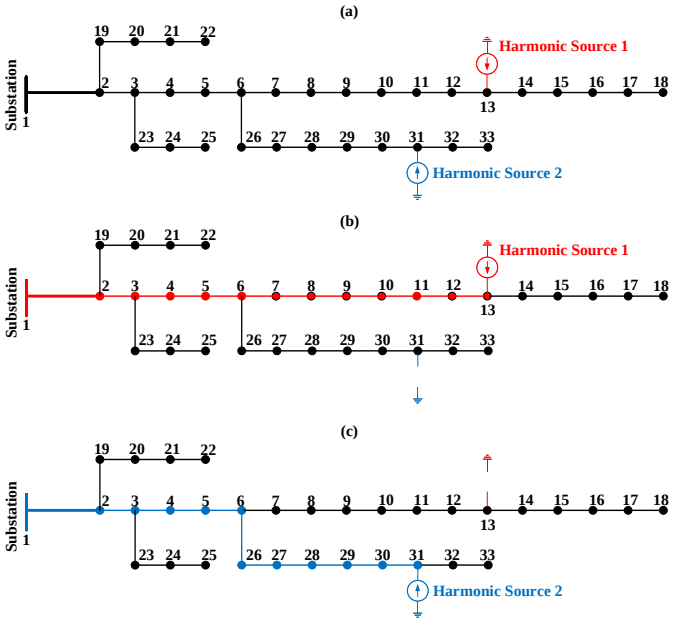

Fig. 2. An example distribution feeder with multiple harmonic source. In practice, the harmonic current almost entirely flows through the substation.

IV. Physics-Aware HSE Solution: Multiple Harmonic Sources

The MIQP formulation in (17) fully incorporates the fundamental physics-based concepts that we discussed in Section III-A. However, a key assumption in (17) is that there is only *one* harmonic source in the network. This assumption may *not* always hold in practice. Therefore, in this section, we properly extend the proposed physics-aware HSE solution to the case where there are *multiple* harmonic sources in the network.

If each of the harmonic sources in the network has a *different* harmonic order, then we can simply solve the optimization problem in (17) for *each* harmonic order *separately*. In such cases, the HSE problem reduces to the same analysis as in Section III. Therefore, for the rest of this section, we rather focus on the more challenging case where there exist multiple harmonic sources of the *same* harmonic order.

Throughout this section, we assume that the number of harmonic sources is known; but their locations are unknown. The case in which neither the number nor the locations of the harmonic sources are known will be discussed in Section V.

A. Decomposition of the Problem

To address the case with multiple harmonic sources, we apply the *superposition theorem* from Circuit Theory [38]. We decompose the HSE problem and introduce a separate set of state variables corresponding to each harmonic source based on a separate equivalent circuit. Once the harmonic voltage phasors and the harmonic current phasors are defined separately in accordance to each individual harmonic source and its corresponding equivalent circuit, we can algebraically add them together in order to obtain the overall harmonic state variables for the understudy power distribution system.

An example is shown in Fig. 2. First, consider the power distribution feeder in Fig. 2(a), which has two harmonic

sources of the same harmonic order at buses 13 and 31. Each harmonic source injects a certain level of harmonic current to the network. Based on the superposition theorem, we can decompose the analysis of this circuit into two separate cases, one based on the analysis of *only* the harmonic source at bus 13; see Fig. 2(b), and another one based on the analysis of *only* the harmonic source at bus 31; see Fig. 2(c). Similar to the discussion in Section III-A, the injected current from each of the two harmonic sources flows through its associated substation connector path, as marked on Figs. 2(b) and (c), respectively. If we denote the vector of the state variables corresponding to the decomposed circuit for the first harmonic source by $\mathbf{X}_1(h)$ and the vector of the state variables corresponding to the decomposed circuit for the second harmonic by $\mathbf{X}_2(h)$, then from the superposition theorem, we know that:

$$\mathbf{X}(h) = \mathbf{X}_1(h) + \mathbf{X}_2(h); \tag{18}$$

where $\mathbf{X}(h)$ is the vector of state variables for the original circuit, i.e., the one that has multiple harmonic sources.

We can similarly break down any power distribution circuit with multiple harmonic sources to a superposition of multiple decomposed circuits; thus solving the HSE problem separately for each harmonic source; and then adding up the results. This approach is explained in details in the next subsection.

B. Extended Physics-Aware MIQP Formulation

For a given harmonic order h, suppose there are $K(h)$ harmonic sources across the distribution feeder. Let us define:

$$\mathcal{K}(h) = \{1; \ldots; K(h)\}: \tag{19}$$

Based on our discussion in the previous section, let us apply the superposition theorem and decompose the distribution feeder into $K(h)$ circuits such that in each of them only one of the harmonic sources is present and the rest are eliminated. For each $b \in \mathcal{K}(h)$, let $\mathbf{X}_b(h)$ denote the vector of state variables for the decomposed circuit by the superposition theorem that corresponds to the b-th harmonic source:

$$\mathbf{X}_b(h) = [(\mathbf{I}_{N;b}(h))^\top (\mathbf{I}_{L;b}(h))^\top (\mathbf{V}_b(h))^\top]^\top: \tag{20}$$

We can expand the summation in (18) to have:

$$\mathbf{X}(h) = \sum_{b \in \mathcal{K}(h)} \mathbf{X}_b(h): \tag{21}$$

Similar to (12), for each decomposed circuit, we know that only one harmonic source is present. Therefore, we have:

$$\mathbf{1}^T \mathbf{b}_b = 1; \quad \forall b \in \mathcal{K}(h): \tag{22}$$

Furthermore, similar to (13)-(16), we know that the following equations hold for each set of state variables associated with each of the decomposed circuits for each harmonic source:

$$\mathbf{I}_{N;b}(h) \geq \mathbf{M}\mathbf{b}_b; \quad \forall b \in \mathcal{K}(h); \tag{23}$$

$$\mathbf{I}_{N;b}(h) \leq \mathbf{M}\mathbf{b}_b; \quad \forall b \in \mathcal{K}(h); \tag{24}$$

$$\mathbf{A}\mathbf{I}_{L;b}(h) \geq \mathbf{M}(\mathbf{1} - \mathbf{b}_b); \quad \forall b \in \mathcal{K}(h); \tag{25}$$

$$\mathbf{A}\mathbf{I}_{L;b}(h) \leq \mathbf{M}(\mathbf{1} - \mathbf{b}_b); \quad \forall b \in \mathcal{K}(h); \tag{26}$$

$$\mathbf{B}\mathbf{V}_b(h) \geq \mathbf{M}(\mathbf{1} - \mathbf{b}_b); \quad \forall b \in \mathcal{K}(h); \tag{27}$$

$$\mathbf{B}\mathbf{V}_b(h) \leq \mathbf{M}(\mathbf{1} - \mathbf{b}_b); \quad \forall b \in \mathcal{K}(h): \tag{28}$$

Matrices $\mathbf{A}$, $\mathbf{B}$, $\mathbf{M}$, and $\mathbf{1}$ do *not* have superscript h; because they do not depend on the number of harmonic sources.

We can now MIQP formulation in (17) to the case with the presence of multiple harmonic sources as follows:

$$\underset{\substack{\mathbf{x}(h);\mathbf{x}_b(h);\mathbf{b}_b \\ \forall b \in \mathcal{K}(h)}}{\textbf{minimize}} \quad \left\| \begin{bmatrix} \mathbf{Z}(h) & \mathbf{H}(h) \\ \mathbf{0} & \mathbf{G}(h) \end{bmatrix} \mathbf{X}(h) \right\|_2^2 \tag{29}$$

$$\textbf{subject to} \quad \text{Eqs. (1); (20) (28):}$$

The above optimization problem incorporates all the harmonic sources into one integrated formulation. Note that, the optimization variables corresponding to all the harmonic sources are *coupled* through the constraints in (21); therefore, they all simultaneously affect the objective function in (29).

In each binary vector $\mathbf{b}_b$, only one entry is non-zero; which pinpoints the location of the b-th harmonic source. The solution of the optimization problem in (29) gives us the estimation of the state variables for the original circuit, as well as those for all the $K(h)$ decomposed circuits. Just like the problem in (17), the problem in (29) is a MIQP. Hence, it can be solved by using a commercial solver such as CVX [37].

With regards to the complexity of our method, suppose there are $K(h)$ harmonic sources of order h across the distribution feeder. The MIQP HSE formulation in (29) would include $K(h)(2|\mathcal{N}| + |\mathcal{L}|)$ continuous variables (corresponding to harmonic state variables) and $K(h)|\mathcal{N}|$ binary variables (corresponding to the harmonic sources to be identified).

Importantly, if the binary variables are relaxed, then the MIQP optimization in (29) becomes a convex optimization problem. Therefore, the complexity of the method primarily depends on the number of binary variables, i.e., $K(h)|\mathcal{N}|$.

V. Physics-Aware HSE Solution: Unknown Number of Harmonic Sources

So far, we have assumed that the number of harmonic sources, i.e., $K(h)$ is known to us. The final step to complete our design in this paper is to relax such assumption. In this section, we assume that $K(h)$ is *not* known. Instead, it needs to be estimated. This can be done by using a novel algorithm, as shown in Algorithm 1. This algorithm is based on conducting an exhaustive search. The key in this algorithm is the *for loop* from Line 4 to Line 12. At first, we assume that there is only one harmonic source in the system, i.e., $K = 1$, and we solve the HSE problem in (29). Next, we set $K = 2$ and solve (29) again. Every time we do so, a new non-zero entry is obtained in vector $\mathbf{I}_N(h)$, while the value and the location of the previous non-zero entries may also change.

What matters to us in this exhaustive search is the value of the smallest non-zero entry in the vector of harmonic nodal injection current phasors, i.e., $\mathbf{I}_N(h)$. Let $\mathbf{I}_N^{\neq 0}(h)$ denote the vector which includes only the non-zero entries of vector $\mathbf{I}_N(h)$. In every iteration that we solve the HSE problem, we check to see if the following condition holds:

$$\min \left\{ \left| \mathbf{I}_N^{\neq 0}(h) \right| \right\} \leq \varepsilon; \tag{30}$$

where ε is a predefined threshold which is selected based on the smallest harmonic current magnitude that we are concerned

Algorithm 1 HSE in low-Observable distribution network with *unknown* number and location(s) of harmonic source(s)

Set threshold .
Set $\mathsf{X}(h) = 0$.
Set $K(h) = fg$.
for $K = 1$ to $jNj \quad 1$ **do**
  Solve Problem (29) to obtain $\mathsf{X}(h)$.
  if condition (30) holds **then**
    $\mathsf{X}(h) = \mathsf{X}(h)$;
    $K(h) = f1;:::;Kg$.
  else
    break;
  end if
end for

about in practice for nodal injection by a harmonic source. If the inequality in (30) does *not* hold, then it means that we have already passed the actual number of harmonic sources; and the value of K in the *previous* iteration is the true number. Once the algorithm ends it returns the number of harmonic sources as well as the ultimate results for harmonic state estimation.

As a special case, if there is *no* harmonic source in the network, then the algorithm ends *without* changing the initial values for $\mathsf{X}(h)$ and $\mathsf{K}(h)$. Accordingly, the outcome of Algorithm 1 is correct even under such special case.

VI. Placement of H-PMUs

In this paper, we assume that only very few H-PMUs are available. Therefore, low-observability is the primary challenge, *regardless* of *where* the H-PMUs are located. Thus, sensor placement is *not* the focus of this paper. Instead, we assume that the H-PMUs are already installed at very few locations; and we rather focus on solving the HSE problem to cope with the low-observability issues. It should be added that, in this work, H-PMUs are assumed to be installed at only 15% 25% of the buses. For instance, for the IEEE 33-bus test network that we will discuss in Section VII-D, only six buses (i.e., only 18% of the buses) are assumed to have H-PMUs.

Nevertheless, in this section, we provide some discussions on the subject of sensor placement to serve as a supplementary insight. First, we discuss the intuitive importance of certain locations to install H-PMUs on a radial topology. Next, we provide an algorithm to select the locations of the H-PMUs.

A. Intuitive Importance of Certain Buses to Host H-PMUs

Let us again consider the IEEE 33-bus test network. We can distinguish *three groups* of buses, as marked on Fig. 3: 1) The buses that are circled in red, which include the substation and all the terminal buses, i.e., buses 1, 18, 22, 25, and 33. 2) The buses that are circled in blue, which are at the head of laterals, i.e., buses 2, 3, and 6. 3) The rest of the buses.

The buses in Group 1, i.e., those that are circled in red, are particularly beneficial to host H-PMUs. The intuitive reason is that, if we place H-PMUs at the buses in Group 1, then *every* bus in the system is monitored by at least a pair of an *upstream* sensor and a *downstream* sensor. The advantage of

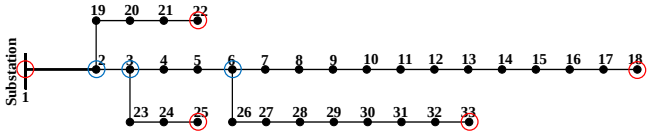

Fig. 3. Three groups of buses on a radial feeder: 1) the buses that are circled in red, 2) the buses that are circled in blue, and 3) the rest of the buses.

such dual monitoring has been reported also in prior studies, e.g., in [39]. Further, as we will see in a case study in Section VII-F, moving H-PMUs away from the buses in Group 1 leads to degradation in the HSE performance, depending on how far we move the H-PMUs away from the buses in Group 1.

The buses in Group 2, i.e., those that are circled in blue, are also (to a lesser extent) beneficial to host H-PMUs. For example, by placing an H-PMU at bus 6, we can enhance the *upstream* monitoring of the buses on two major branches of the radial network topology, i.e., for buses 7 to 18 on the main as well as for buses 26 to 33 on a lateral; while we also enhance the *downstream* monitoring of buses 2 to 5.

From the above intuitive explanations, and given the fact that our focus in this paper is on low-observable power networks with very few H-PMUs, we expect that the choices of the H-PMUs should include the buses in Group 1 and possibly a few buses in Group 2. Nevertheless, the main challenge remains to be the issue of low-observability in the system.

B. H-PMU Placement based on Algorithm

Further to the intuitive approach in Section VI-A, next, we provide an algorithm to choose the locations of H-PMUs based on the desired number of H-PMUs. This algorithm is provided to make the paper self-sufficient. Please refer to the very rich literature in this field, such as in [27]–[30], for more details.

In the proposed sensor placement algorithm, we start from the case where *all* buses are equipped with an H-PMU, i.e., we start with the hypothetical case where the power distribution network has full observability. Then, in every iteration, we seek to remove *one* of the H-PMUs such that we experience the lowest decline in the accuracy of the proposed HSE method after solving the optimization problem in (17). Here, we examine the hypothetical presence of the harmonic source at each bus and consider the *average* of the resulting MSE values. After we remove one H-PMU, we repeat this process to remove H-PMUs one by one, until we reach the desired number of installed H-PMUs. Please note that, due to the radial topology of the network, it might happen in some iterations that removing an H-PMU from a group of neighboring buses leads to an *equal* amount of decline in the MSE. In that case, one can remove the H-PMU from either one of those buses. In such rare cases, instead of removing one of the identified buses randomly, we rather follow our intuitive discussion in Section VI-A and we give the priority to keep the H-PMUs at buses in Group 1 over Group 2, and Group 2 over Group 3. The summary of the above process is shown in Algorithm 2.

VII. Case Studies

In this section, we examine different case studies based on the IEEE 33-Bus test network [40]. We run the har-

TABLE I
PERFORMANCE COMPARISON BETWEEN DIFFERENT HSE METHODS

Method	K = 1		K = 2		K = 3		K = 4		K = 5	
	MSE V	MSE I	MSE V	MSE I	MSE V	MSE I	MSE V	MSE I	MSE V	MSE I
Proposed Method	0.0156	0.0019	0.8578	0.2447	0.9714	0.1383	1.7510	0.2646	25.226	9.948
[13]	201.72	4.202	408.06	13.21	971.04	20.922	1790.1	41.176	1993.2	63.66
[15]	202.21	8.71	417.33	31.89	1935.31	43.78	1879.47	78.45	2007.9	125.6

Algorithm 2 Placement of H-PMUs

The desired total number of available H-PMUs is P.
Initially, place H-PMU at every node, i.e., $M = N$
Set $M = fg$
for $m = 1$ to $jNj \quad P$ **do**
  minMSE = 1e3
  $F = \{\}$
  for $i \; 2 \; M = M$ **do**
    Remove H-PMU at bus i and Solve Problem (17).
    if MSE < minMSE **then**
      minMSE = MSE;
      $F = \{i\}$
    end if
  end for
  Set $M = M \quad [F$
end for
Return $M \quad M$

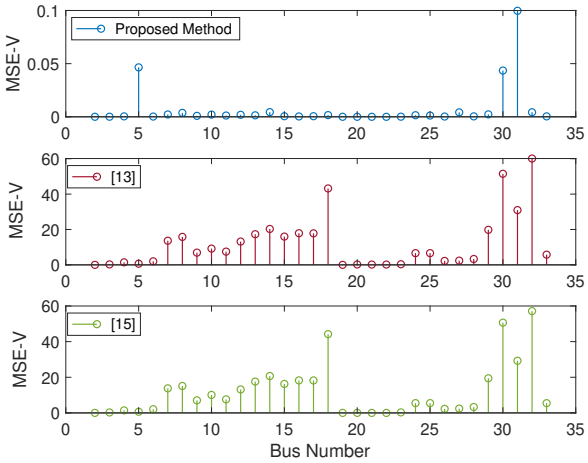

Fig. 4. MSE in estimating harmonic voltage phasors at all buses, for three different methods, versus the location of the harmonic source. The number of harmonic sources is $K = 1$. The harmonic order is $h = 3$.

monic power flow in the Open Distribution System Simulator (OpenDSS) [41], and then we use CVX toolbox with MOSEK solver [37] in MATLAB to solve the HSE optimization problem in (29) and to execute the steps in Algorithm 1.

Unless stated otherwise, we assume that six H-PMUs are installed on the network and measure the harmonic nodal voltage phasors and the harmonic line current phasors.

The placement of the H-PMUs is done by Algorithm 2, where the desired number of H-PMUs is $P = 6$. Accordingly, H-PMUs are installed at buses 1, 6, 18, 22, 25, and 33.

We assume that up to five harmonic sources may exist on the power distribution feeder, and they may inject harmonic currents with harmonic orders $h = 3$, 5, and 7. The magnitude of the harmonic source at a bus is assumed to be up to 30% of the default load at that bus in the IEEE 33-Bus test feeder.

A. Performance Comparison

We compare the performance of our method with two other methods. We choose the methods in [13] and [15] for the purpose of performance comparison. The method in [13] is based on some popular sparse recovery techniques. It works by considering the nodal injection currents as the vector of state variables. Sparse recovery is done by conducting an ℓ_1-norm minimization. Therefore, this method is inherently designed to solve the HSE problem under the low-observability condition without the need for making any modifications. As for the method in [15], it is based on Singular Value Decomposition (SVD). It has some structural characteristics which can be used to solve an undetermined system of equations. This method addresses *low-observability* by examining singular values and the null space vectors of the measurement matrix.

As the metric for performance comparison, we use the Mean Square Error (MSE) in the HSE results. Since the magnitudes of the harmonic voltage phasors are different from the magnitudes of the harmonic current phasors, we calculate the MSE for each type of harmonic variables separately. Thus, we provide separate results for MSE V and MSE I.

The results are shown in Table I. Here the harmonic source is at harmonic order $h = 3$ and the magnitude of the injected harmonic current is 30% of the default load of the bus where the harmonic source is located. As we can see, the MSE for both voltage and current is significantly lower for the proposed method in comparison with the methods in [13] and [15]. Of course, as we increase the number of harmonic sources, the MSE increases in all three methods. However, in all cases, the proposed physics-aware method performs drastically better.

Another comparison between the performance of the proposed method and those of [13] and [15] is done is Fig. 4. Here we examine the MSE V for each of the three methods versus the location of a single harmonic source. The harmonic source is at harmonic order $h = 3$, and the magnitude of the injected harmonic current is 10% of the default load at each bus where the harmonic source is located. As it can be seen in Fig. 4, the proposed method demonstrates a much lower MSE in comparison with the works in [13] and [15].

B. Harmonic Source Location Identification

Although the focus in this paper is on harmonic state estimation, it is worth to also compare our proposed method

TABLE II
PERFORMANCE OF ALGORITHM 1 IN IDENTIFYING THE LOCATIONS OF HARMONIC SOURCES AT BUSES 14, 21, 24, 29

K	Optimal Objective Value	$\mathbf{I}_N^{\neq 0}(h)$	Identified Buses in $\mathcal{K}^*(h)$	Condition (30) Holds
1	49.031	[**15.6116**]	4	Yes
2	22.048	[5.5396, **2.8066**]	9,**24**	Yes
3	15.636	[2.841, 3.2957, **1.3907**]	13,30,**24**	Yes
4	0.282	[2.4905, **0.5127**, 3.2778, 1.6933]	14,**21**,24,29	Yes
5	0.236	[2.4767, **0.0054**, 0.5127, 3.2791, 1.6964]	14,**18**,21,24,29	**No**

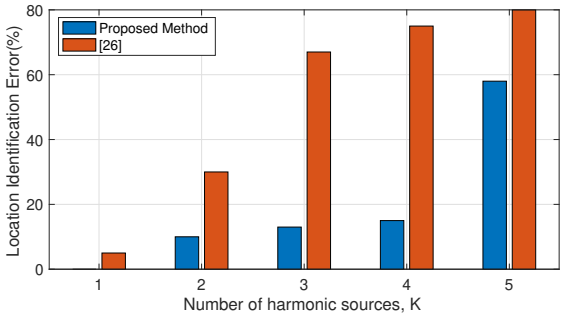

Fig. 5. Error in location identification of the harmonic source(s).

with the existing methods that are designed to identify the location(s) of harmonic source(s). In any such comparison, we would utilize only a subset of the strengths of our proposed method. Clearly, not every HSE method can also identify the unknown location(s) and the unknown number of the harmonic source(s). However, the approach in this paper *does* provide the number and the location(s) of the harmonic source(s) as a *bi-product* of the proposed physics-aware MIQP HSE method. Therefore, making such comparison could be insightful.

In this case study, we compare the average error in identifying the location(s) of harmonic source(s) of the proposed method versus the method in [26], which is designed to identify the location(s) of the harmonic source(s). The harmonic source location identification method in [26] is based on the concept of compressed sensing. The results are shown in Fig. 5. As the number of harmonic sources increases, it causes degradation in the performance of both methods. However, the proposed HSE method demonstrates a better performance in all scenarios. Of course, unlike our proposed method, the method in [26] does *not* also solve the harmonic state estimation problem, as it is *not* designed to do so.

C. Performance of Algorithm 1 in Scenarios with Unknown Number and Location(s) of Harmonic Source(s)

In this section, we investigate the performance of Algorithm 1 in correctly estimating the *number* of harmonic sources as well as the *location(s)* of the harmonic sources.

Suppose there are four harmonic sources at buses 14, 21, 24, and 29. All harmonic sources are at the same harmonic order, where $h = 3$. We assume that neither the number nor the locations of the harmonic sources are known.

Table II shows several details about the operation of Algorithm 1 for the above scenario. At each step of the *for loop* in Algorithm 1, this table shows several details about the internal parameters in the algorithm. The first column denotes the value of parameter K. The second column denotes the optimal objective value of the optimization problem in (29). The third column shows the entries in vector $\mathbf{I}_N^{\neq 0}(h)$, i.e., the non-zero entries in vector $\mathbf{I}_N(h)$. The number in bold is the entry that has the smallest amount, i.e., the entry that is corresponding to the condition in (30). The fourth column shows the current list of buses in set $\mathcal{K}$. The number in bold is the bus number that is corresponding to the condition in (30). The fifth column indicates whether condition (30) holds; 'Yes' means condition (30) holds; and 'No' means condition (30) does not hold. Parameter in (30) is set to 0.01.

Per Algorithm 1, we continue incrementing K for as long as condition (30) holds. Accordingly, the highest value of K for which condition (30) holds gives us the number of harmonic sources in the network. For the example, in Table II, the number of harmonic sources is obtained as $K = 4$, which is correct. If we consider $\mathcal{K}(h)$ at the row corresponding to $K = 4$, it gives us the locations of all harmonic buses:

$$\mathcal{K}(h) = \{14, 21, 24, 29\}, \tag{31}$$

which is indeed correct; because the harmonic sources are indeed at buses 14, 21, 24, and 29. Notice that, for the last row in Table II, that is corresponding to $K = 5$, bus 18 is *not* a correct location for a harmonic source. Its corresponding value in vector $\mathbf{I}_N^{\neq 0}(h)$ is 0.0054, which is *less* than $= 0.01$; hence, the condition in (30) does *not* hold at $K = 5$.

It is worth mentioning that, the optimal objective value, i.e., the value in the second column in Table II, is non-increasing in terms of parameter K; it cannot increase as we increase K.

D. Increasing the Number of Harmonic Sources

Recall from Table I that increasing the number of harmonic sources (of the same harmonic order) makes the HSE problem more challenging. It is very challenging to solve the HSE problem when 1) there are several harmonic sources in the network, 2) the number of the harmonic sources is unknown, 3) the locations of the harmonic sources is unknown, and 4) we have only a few sensors deployed on the network. However, as we will show in this section, the performance of Algorithm 1 can improve by slightly increasing the number of H-PMUs.

Here, we examine a total of 100 random scenarios, where the randomness is with respect to the locations and the magnitudes of the harmonic sources. Our goal is to examine the percentage of the harmonic sources whose locations are identified correctly (or almost correctly). The results are shown in Fig. 6. In each bar, the dark portion indicates the cases where the exact bus is identified while the light portion

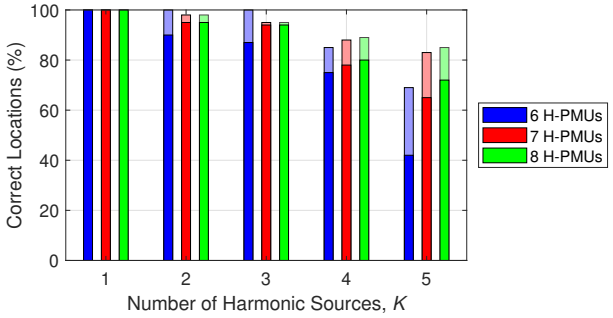

Fig. 6. The impact of increasing the number of H-PMUs on improving the performance of Algorithm 1 in identify the locations of the harmonic sources as we increase the number of harmonic sources in the network. In each bar, the dark portion indicates the cases where the exact bus is identified while the light portion indicates the cases where the neighboring bus is identified.

indicates the cases where the *immediate neighboring* bus is identified. Therefore, the length of each bar indicates the percentage of the the harmonic sources whose locations are identified either exactly or by only one bus difference.

First, consider the case with the default number of H-PMUs, i.e., when there are six H-PMUs in the system; one at the substation and the others at buses 6, 18, 22, 25, and 33. As we can see, the performance of Algorithm 1 is generally acceptable when K is 1, 2, 3, or 4. However, the performance drops when K is 5. Next, consider the case where the number of H-PMUs is seven. The 7th H-PMU is installed at bus 14. As we can see, the performance of Algorithm 1 improves significantly. In particular, when K is 5, the percentage of the harmonic sources whose locations are identified correctly increases to 65% (exact bus) and 83% (exact or neighboring bus). Finally, consider the case where the number of H-PMUs is eight. The 8th H-PMU is installed at bus 29. As we can see, the performance of Algorithm 1 further improves. In particular, when K is 5, the percentage of the harmonic sources whose locations are identified correctly further increases to 72% (exact bus) and 85% (exact or neighboring bus).

From the results in Fig. 6, we can conclude that, as the number of harmonic sources increases, we would need more H-PMUs to be installed in the system in order to maintain high accuracy in the harmonic state estimation results.

E. Increasing the Harmonic Order

To investigate the effect of harmonic order on the accuracy of the proposed HSE method, we perform a sensitivity analysis based on the harmonic order h, and with respect to different number of harmonic sources K. We compare the results of our method with those of the methods in [13] and [15]. To have a consistent comparison, we assume that the magnitude of the harmonic injection current for different harmonic orders is the same. The magnitude of each harmonic source is 10% of the default load at the bus where the harmonic source is located. The results for the MSE of harmonic nodal voltage phasors and the MSE of harmonic line current phasors are shown in Table III. As we can see, the proposed method demonstrates a drastically better performance compared with [13] and [15].

TABLE III
PERFORMANCE UNDER DIFFERENT HARMONIC ORDERS

K	h	MSE V			MSE I		
		Proposed Method	[13]	[15]	Proposed Method	[13]	[15]
1	3	0.0017	1.25	7.02	0.00025	0.94	0.83
	5	0.0046	1.96	17.3	0.00028	1.17	1.29
	7	0.0089	2.63	32.9	0.00035	1.37	1.94
2	3	0.0030	3.91	18.3	0.00037	1.65	2.20
	5	0.0077	6.28	40.8	0.00049	2.10	3.39
	7	0.0153	8.35	100	0.00060	2.43	4.36
3	3	0.0052	6.40	30.9	0.00077	2.25	3.42
	5	0.0323	10.1	74	0.00858	2.84	5.29
	7	0.1075	13.1	134	0.01467	3.28	6.81
4	3	0.0718	11.9	101	0.00970	3.20	4.80
	5	0.0917	19.1	141	0.01050	4.08	7.40
	7	0.1590	24.7	202	0.02150	4.60	10.1

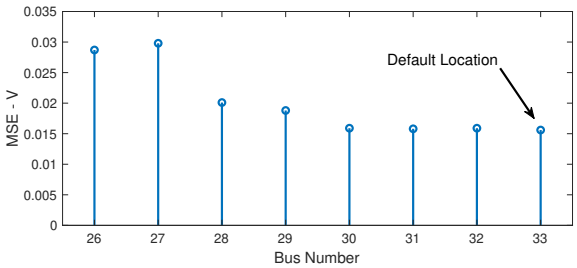

Fig. 7. The impact of changing the location of one of the H-PMUs.

F. Impact of Changing the Location of H-PMUs

As it was mentioned in Section I-B, sensor placement is beyond the scope of this paper. Nevertheless, it is interesting to examine the sensitivity of our proposed method to changing the location of an H-PMU. Thus, in this section, we examine the results when we change the location of the H-PMU that is at bus 33. Here, we move the sensor to every bus on an entire lateral that includes buses 26 to 33. The results are shown in Fig. 7. As we can see, the performance of the method, i.e., the MSE index, remains almost unchanged as we move up to three buses away from the default location of the sensor at the end of the lateral. However, if we move away even further, then we gradually start experiencing degradation in the performance. We can conclude that, the best option is to stick to the typical placement of the sensors as in the aforementioned default setting. Nevertheless, we can see that the proposed method is not very sensitive to the exact location of the H-PMUs, and it may cope with slight changes in the location of the sensors.

G. Impact of Unbalanced Operation

Next, we study the impact of having unbalanced phases on the performance of the proposed HSE method. In this case study, we examine a larger power distribution network, namely the IEEE 123 bus test system [42]. The majority of the loads in this test system are single phase loads that are on different phases. There are also multiple unbalanced three-phase loads with Wye connections. Many of the laterals in this network are very small. We aggregate the loads on any such small lateral as a single load point, as shown in red in Fig. 8. We assume that there are only four H-PMUs available, one at the

TABLE IV
PERFORMANCE IN AN UNBALANCED NETWORK

K	MSE V	MSE I
1	0.0183	0.0042
2	0.9174	0.2315
3	1.1289	0.1507
4	2.3154	0.4538
5	29.258	12.743

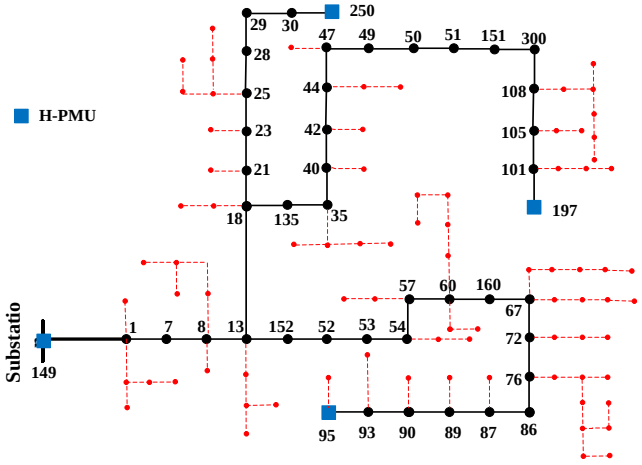

Fig. 8. An example three-phase distribution feeder with unbalanced loads. Four H-PMUs are available at buses 95, 149, 197, and 250.

substation and three at buses 95, 197 and 250. These H-PMUs provide *three-phase* harmonic voltage phasor measurements and *three-phase* harmonic line current phasor measurements. The harmonic source is at harmonic order $h = 3$ and the magnitude of the injected harmonic current is 30% of the default load at the bus where the harmonic source is located.

The results of applying the proposed HSE method are shown in Table IV. By comparing the results in this table and those in Table I, we can see that the performance of the proposed method remains satisfactory despite the phase unbalance in the system. This is because the unbalanced operation of the power distribution system does not change the nature of the problem, such as the characteristics of the substation connector path or the inherent linearity in the equations that directly comes from the Ohm's law. The proposed HSE method works well whether or not the network is balanced.

H. Performance in the Presence of DERs

In this Section, we evaluate the performance of our method in the presence of distributed energy resources (DERs). The results are shown in Table V. Here, we assume that five DERs are at buses 5, 15, 20, 24, and 29. We consider different scenarios for different number of harmonic sources. All harmonic sources are at harmonic order $h = 3$ and the magnitude of the injected harmonic current is 30% of the default load at the bus where the harmonic source is located. As we can see in Table V, our method demonstrates similar accuracy as the previous case, where there were no DERs, such as in the results in Table I. The reason is that, the presence of DERs does *not* impact the sparsity patterns that we extracted in Section III. Also, it is worth mentioning that DERs may cause reverse power flow on the fundamental component of the current [8]; however, our focus in this paper is rather on the harmonic components, not the fundamental component.

TABLE V
PERFORMANCE IN THE PRESENCE OF DERS

	K =1	K = 2	K = 3
MSE - V	0.0158	0.8913	0.9937
MSE - I	0.0025	0.2562	0.1443

I. Validation of the Superposition Theorem

We end the case studies by directly examining and validating the application of the superposition theorem in our proposed HSE method. Same as in Section VII-C, suppose there are four harmonic sources at buses 14, 21, 24, and 29.

For the purpose of this validation task, we run the harmonic power flow for four different cases. In each case, exactly one of the four harmonic sources is assumed to be connected to the network, while the remaining three harmonic sources are disconnected. Furthermore, we also separately run the harmonic power flow for the case that *all four* of the harmonic sources are connected to the network.

Let us denote the vector of the harmonic line current phasors corresponding to the first four cases by $\mathbf{I}_{L;1}$, $\mathbf{I}_{L;2}$, $\mathbf{I}_{L;3}$, and $\mathbf{I}_{L;4}$. They are corresponding to the simulation of the four cases with individual harmonic sources, i.e., when the only harmonic source in the network is at bus 14, at bus 21, at bus 24, and at bus 29, respectively. If the superposition theorem holds, then the following summation:

$$\mathbf{I}_{L;1} + \mathbf{I}_{L;2} + \mathbf{I}_{L;3} + \mathbf{I}_{L;4}; \tag{32}$$

would closely match $\mathbf{I}_L$ which is the harmonic current phasor corresponding to the case where all four harmonic sources are connected to the network. This issue is validated in Fig. 9. As we can see, there is almost a perfect match between the summation in (32), which is the outcome of applying the superposition theorem, and the actual simulation results with the simlultanous presence of all four harmonic sources.

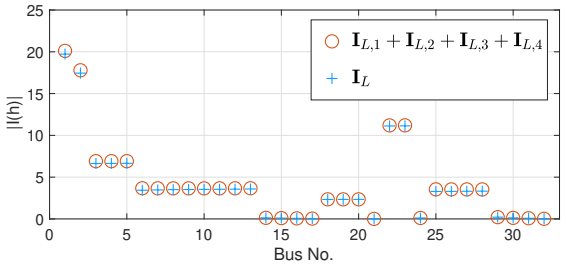

Fig. 9. An illustrative example to validate the superposition theorem among the harmonic state variables. There are four harmonic sources on the network.

VIII. CONCLUSIONS

A novel physics-aware MIQP formulation as well as corresponding innovative algorithm were proposed in order to solve the harmonic state estimation in low-observable power

distribution feeders. In this method, based on analyzing the physical characteristics of the network, we first extract the sparsity patterns of the harmonic state variables in the presence of a single harmonic source. Next, we focus on the more practical cases, where there are multiple harmonic sources on the network, and the number and the location(s) of the harmonic sources are *unknown*. Accordingly, we make an innovative use of the superposition theorem and develop a methodology to obtain the number and location(s) of the harmonic sources through the integrated process that also simultaneously addresses harmonic state estimation. The methodology in this paper is unique. It not only addresses a highly challenging problem, it also introduces a new application for H-PMUs, which are an emerging class of smart grid sensors. The effectiveness of the proposed method was verified through various case studies and compared with the existing methods.

APPENDIX A

In this Appendix, we explain how to construct matrices $\mathbf{H}(h)$ and $\mathbf{G}(h)$ in order to formulate the equation in (5).

The measurement matrix $\mathbf{H}(h)$ contains two types of rows. The first type of rows in matrix $\mathbf{H}(h)$ is associated with harmonic voltage phasor measurements. The following relationship holds between the harmonic nodal injection current phasors and the harmonic voltage phasor measurements:

$$\mathbf{V}^m(h) = \mathbf{U}_V^m \mathbf{Y}^{-1}(h)\, \mathbf{I}_N(h); \tag{33}$$

where $\mathbf{U}_V^m \in \mathbb{R}^{jNj \times jNj}$ is a diagonal matrix,such that its diagonal entry in row i is 1 if the associated bus i is equipped with measurement, and otherwise it is zero. Also, $\mathbf{Y}(h)$ is the admittance matrix for harmonic order h. In addition to (33), the harmonic voltage phasor measurements can be mapped also to their associated entries in the vector of harmonic voltage phasors through an identity mapping:

$$\mathbf{V}^m(h) = \mathbf{U}_V^m\, \mathbf{V}(h); \tag{34}$$

The second type of rows in matrix $\mathbf{H}(h)$ is associated with the harmonic line current measurements. The harmonic line current measurements are mapped to the vector of harmonic nodal voltage phasors as follows:

$$\mathbf{I}_L^m(h) = \mathbf{U}_I^m \mathbf{Y}_{\text{prim}}(h)\, \mathbf{V}(h); \tag{35}$$

where $\mathbf{U}_I^m \in \mathbb{R}^{jLj \times jLj}$ is a diagonal matrix, such that its diagonal entry in row i is 1 if the associated line segment i is equipped with measurement, and otherwise it is zero. Also, $\mathbf{Y}_{\text{prim}}(h)$ is the primitive admittance matrix [43], which includes the line admittances only for the line segments whose harmonic current phasors are measured. Harmonic line current phasor measurements can also be related to the vector of the harmonic line current phasors through an identity mapping:

$$\mathbf{I}_L^m(h) = \mathbf{U}_I^m\, \mathbf{I}_L(h); \tag{36}$$

As for matrix $\mathbf{G}(h)$, it includes similar equations to (35). But for the line segments that are *not* equipped with H-PMUs, we use an equation that captures the relationship between the harmonic nodal voltage and the harmonic line currents:

$$\mathbf{0} = (\mathbf{I} - \mathbf{U}_I^m)(\mathbf{Y}_{\text{prim}}(h)\, \mathbf{V}(h) - \mathbf{I}_L(h)); \tag{37}$$

where $\mathbf{I} \in \mathbb{R}^{jLj \times jLj}$ is an identity matrix. The equations in (37) create more coupling among the state variables, which finally appears in (5) as:

$$\mathbf{0} = \mathbf{G}(h)\mathbf{X}(h); \tag{38}$$

It is worth mentioning that, for a network with low observability, it is crucial to use the augmented formulation in (5) in order to at least *include* the *unobservable* harmonic variables in the equations of the *HSE problem* formulation through the use of matrix $\mathbf{G}(h)$. Otherwise, there is no other place to include the unobservable harmonic variables in the formulation of the problem; which would *not* allow estimating them.

APPENDIX B

In this Appendix, we explain the key characteristics of the *substation connector path* that was mentioned in Section III-A. In particular, we explain why the harmonic current *almost entirely* flows through the substation, i.e., through the substation connector path, which is marked in red in Fig. 1. The steps to explain this concept are shown in Fig. 10.

First, consider the network model in Fig. 10(a). Here, we have replaced the laterals with their equivalent impedance. In particular, we have replaced the lateral that contains buses 19 to 22 with impedance $Z_{19\ 22}$; the lateral that contains buses 23 to 25 with impedance $Z_{23\ 25}$; and the lateral that contains buses 26 to 33 with impedance $Z_{26\ 33}$. Furthermore, we replaced the part of the main feeder that is on the *right hand side* of the harmonic source at bus 13, i.e., the part that includes buses 14 to 18, with impedance $Z_{14\ 18}$. As for Z_{Thevein}, it denotes the impedance in the Thevenin equivalent of the substation that is seen by the distribution feeder.

In Fig. 10(a), since Z_{Thevein} and $Z_{19\ 22}$ are in parallel; and because, in practice, the impedance of the power network as seen at the substation is much smaller than the impedance of any lateral [44], i.e., Z_{Thevenin} is much smaller than $Z_{19\ 22}$, we can conclude that no harmonic current will go through $Z_{19\ 22}$. Instead, almost the entire harmonic current will go through the substation. Therefore, we can eliminate the lateral and reduce the network model to Fig. 10(b).

Similarly, in Fig. 10(b), since Z_{Thevenin} and $Z_{23\ 25}$ are in parallel, and Z_{Thevenin} is much smaller than $Z_{23\ 25}$, we can conclude that no harmonic current will go through $Z_{23\ 25}$. Note that, with a slight abuse of notation, Z_{Thevenin} in Fig. 10(b) is redefined as the impedance of the Thevenin equivalent of the *combination* of the substation and bus 2. We can eliminate the lateral and reduce the network model to Fig. 10(c).

Similarly, in Fig. 10(c), since Z_{Thevenin} and $Z_{26\ 33}$ are in parallel, and Z_{Thevenin} is much smaller than $Z_{26\ 33}$, we can conclude that no harmonic current will go through $Z_{26\ 33}$. Therefore, we can eliminate the lateral and reduce the network model to Fig. 10(d). So far, all the laterals are eliminated.

Finally, in Fig. 10(d), since Z_{Thevenin} and $Z_{14\ 18}$ are in parallel, and Z_{Thevenin} is much smaller than $Z_{14\ 18}$, we can conclude that no harmonic current will go through $Z_{14\ 18}$. Therefore, almost the entire harmonic current flows from the harmonic source to the substation through the substation connector path, as it is marked on the figure.

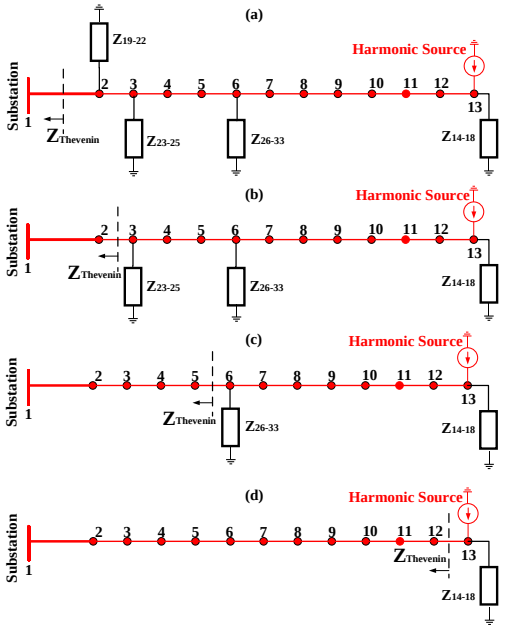

Fig. 10. The illustration of the explanations in the Appendix about the characteristics of the substation connector path: (a) replacing the laterals in Fig. 1 with their equivalent impedances; (b) eliminating the first lateral; (c) eliminating the second lateral; (d) eliminating the third lateral.

APPENDIX C

In this appendix, we explain why it is necessary to consider *both* $\mathsf{V}(h)$ and $\mathsf{I}_L(h)$ as state variables in our HSE problem.

Consider the small network in Fig. 11. The network has five buses. One H-PMU is installed at bus 1 and another H-PMU is installed at bus 5. The H-PMU at bus 1 measures the harmonic nodal voltage phasor at bus 1 and the harmonic line current phasor at line L_1. The H-PMU at bus 5 measures the harmonic nodal voltage phasor at bus 5 and the harmonic line current phasor at line L_4. Accordingly, the vector of harmonic phasor measurements at harmonic order h is:

$$\mathsf{Z}(h) = [V_1(h)^m \;\; V_5(h)^m \;\; I_{L_1}(h)^m \;\; I_{L_4}(h)^m]^\top; \qquad (39)$$

where superscript m indicates a measurement to distinguish the measurements from the state variables. To see the importance of including the line current phasors in the vector of state variables, let us hypothetically assume that we consider *only* the harmonic nodal voltage phasors as state variables:

$$\mathsf{X}(h) = [V_1(h) \; V_2(h) \; V_3(h) \; V_4(h) \; V_5(h)]^\top: \qquad (40)$$

From (3), we would have the following system of equations:

$$\begin{bmatrix} V_1^m(h) \\ V_5^m(h) \\ I_{L_1}(h)^m \\ I_{L_4}(h)^m \end{bmatrix} = \begin{bmatrix} 1 & 0 & 0 & 0 & 0 \\ 0 & 0 & 0 & 0 & 1 \\ y_{L_1}(h) & -y_{L_1}(h) & 0 & 0 & 0 \\ 0 & 0 & 0 & y_{L_4}(h) & -y_{L_4}(h) \end{bmatrix} \begin{bmatrix} V_1(h) \\ V_2(h) \\ V_3(h) \\ V_4(h) \\ V_5(h) \end{bmatrix}. \qquad (41)$$

The above system of equations does not involve $V_3(h)$; because the associated coefficients are zero in all the rows. Thus, it is *impossible* to estimate $V_3(h)$ from the above equations; because $V_3(h)$ is simply *not* part of the equations.

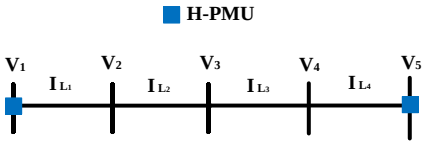

Fig. 11. An illustrative example for the discussion in Appendix C: A small distribution feeder with 5 buses and 4 lines. Only two buses have H-PMUs.

If we do include the harmonic line current phasors in state variables, which is what we do in this paper, we would have:

$$\mathsf{X}(h) = [V_1(h) \;\vdots\; V_5(h) \; I_{L_1}(h) \;\vdots\; I_{L_4}(h)]^\top: \qquad (42)$$

From (5), we would have the following system of equations:

$$\begin{bmatrix} V_1^m(h) \\ V_5^m(h) \\ I_{L_1}(h)^m \\ I_{L_4}(h)^m \\ 0 \\ 0 \end{bmatrix} = [\mathbf{R}] \begin{bmatrix} V_1(h) \\ V_2(h) \\ V_3(h) \\ V_4(h) \\ V_5(h) \\ I_{L_1}(h) \\ I_{L_2}(h) \\ I_{L_3}(h) \\ I_{L_4}(h) \end{bmatrix}, \qquad (43)$$

where

$$\mathsf{R} = \begin{bmatrix} 1 & 0 & 0 & 0 & 0 & 0 & 0 & 0 & 0 \\ 0 & 0 & 0 & 0 & 1 & 0 & 0 & 0 & 0 \\ \frac{y_{L_1}(h)}{2} & \frac{y_{L_1}(h)}{2} & 0 & 0 & 0 & \frac{1}{2} & 0 & 0 & 0 \\ 0 & 0 & 0 & \frac{y_{L_4}(h)}{2} & \frac{y_{L_4}(h)}{2} & 0 & 0 & 0 & \frac{1}{2} \\ 0 & y_{L_2}(h) & y_{L_2}(h) & 0 & 0 & 0 & 1 & 0 & 0 \\ 0 & 0 & y_{L_3}(h) & y_{L_3}(h) & 0 & 0 & 0 & 1 & 0 \end{bmatrix}.$$

The last two rows in (43) are corresponding to matrix $\mathsf{G}(h)$ that we defined in Section II-B. Unlike in (41), the system of equations in (43) involves *all* the state variables. This is a *necessary* condition to estimate all the state variables in the system. This is why we have included the harmonic line current phasors in the vector of the state variables in this paper.

REFERENCES

[1] M. H. Bollen, *Understanding Power Quality Problems*. Wiley-IEEE Press, 2000.

[2] IEEE Standard, "IEEE recommended practices and requirements for harmonic control in electrical power systems," *IEEE Std 519-1992*, pp. 1–112, Apr 1993.

[3] S. Jain, P. Jain, and S. N. Singh, "A fast harmonic phasor measurement method for smart grid applications," *IEEE Transactions on Smart Grid*, vol. 8, no. 1, pp. 493–502, Jan 2017.

[4] A. Carta, N. Locci, and C. Muscas, "A PMU for the measurement of synchronized harmonic phasors in three-piece distribution networks," *IEEE Transactions on Instrumentation and Measurement*, vol. 58, no. 10, pp. 3723–3730, Oct 2009.

[5] B. Zeng, Z. Teng, Y. Cai, S. Guo, and B. Qing, "Harmonic phasor analysis based on improved FFT algorithm," *IEEE Transactions on Smart Grid*, vol. 2, no. 1, pp. 51–59, Mar 2011.

[6] L. Chen, W. Zhao, F. Wang, and S. Huang, "Harmonic phasor estimator for P class phasor measurement units," *IEEE Transactions on Instrumentation and Measurement*, vol. 58, no. 10, pp. 1–10, May 2019.

[7] P. Rodríguez-Pajaró, A. Hernández, and J. V. Milanović, "Estimation of harmonics in partly monitored residential distribution networks with unknown parameters and topology," *IEEE Transactions on Smart Grid (Early Access), doi: 10.1109/TSG.2022.3155976*, pp. 1–14, Mar 2022.

[8] L. Chen, M. Farajollahi, M. Ghamkhari, W. Zhao, S. Huang, and H. Mohsenian-Rad, "Switch status identification in distribution networks using harmonic synchrophasor measurements," *IEEE Transactions on Smart Grid*, vol. 12, no. 3, pp. 2413–2424, May 2021.

[9] I. Molina-Moreno, A. Medina, R. Cisneros-Magaña, O. Anaya-Lara, and J. Salazar-Torres, "Enhanced harmonic state estimation in unbalanced three-phase electrical grids based on the kalman filter and physical scale-down implementation," *International Journal of Electrical Power Energy Systems*, vol. 123, Dec 2020.

[10] R. Cisneros-Magaña, A. Medina, V. Dinavahi, and A. Ramos-Paz, "Time-domain power quality state estimation based on kalman filter using parallel computing on graphics processing units," *IEEE Access*, vol. 6, pp. 21 152–21 163, Apr 2018.

[11] I. Molina-Moreno, A. Medina, R. Cisneros-Magaña, and O. Anaya-Lara, "Time domain harmonic state estimation in unbalanced power networks based on optimal number of meters and the principle of half-wave symmetry," *IET Generation, Transmission Distribution*, vol. 11, no. 15, pp. 3871–3880, Jun 2017.

[12] A. Medina and R. Cisneros-Magaña, "Time-domain harmonic state estimation based on the kalman filter poincare map and extrapolation to the limit cycle," *IET Generation, Transmission Distribution*, vol. 6, no. 12, pp. 1209–1217, Dec 2012.

[13] H. Liao, "Power system harmonic state estimation and observability analysis via sparsity maximization," *IEEE Transactions on Power Systems*, vol. 22, no. 1, pp. 15–23, Feb 2007.

[14] C. F. M. Almeida and N. Kagan, "Harmonic state estimation through optimal monitoring systems," *IEEE Transactions on Smart Grid*, vol. 4, no. 1, pp. 467–478, Mar 2013.

[15] J. Breda, J. Vieira, and M. Oleskovicz, "Three-phase harmonic state estimation for distribution systems by using the SVD technique," in *Power and Energy Society General Meeting (PESGM)*, Jul 2016.

[16] A. Arefi, M. Haghifam, and S. Fathi, "Distribution harmonic state estimation based on a modified PSO considering parameters uncertainty," in *IEEE Trondheim PowerTech*, Sep 2011.

[17] T. Zang, Y. Wang, H. Sun, and Z. He, "Variable parameter kalman filter based dynamic harmonic state estimation for power systems with wind energy integration," in *Proc. of the IEEE Conference on Energy Internet and Energy System Integration*, Nov 2017.

[18] W. Zhou, O. Ardakanian, H. Zhang, and Y. Yuan, "Bayesian learning-based harmonic state estimation in distribution systems with smart meter and DPMU data," *IEEE Transactions on Smart Grid*, vol. 11, no. 1, pp. 832–845, Jan 2020.

[19] D. Bhujel, N. Watson, and T. Jalal, "Application of harmonic state estimation to a distribution system," in *IEEE PowerTech*, Manchester, UK, Jul 2017.

[20] I. D. Melo, J. L. R. Pereira, A. M. Variz, and P. A. N. Garcia, "Harmonic state estimation for distribution networks using phasor measurement units," *Electric Power Sys. Research*, vol. 147, pp. 133–144, Jun 2017.

[21] F. Xu, C. Wang, K. Gue, Q. Shu, Z. Ma, and H. Zheng, "Harmonic sources' location and emission estimation in underdetermined measurement system," *IEEE Transactions on Instrumentation and Measurement, (Early Access), doi: 10.1109/TIM.2021.3077658*, vol. 70, May 2021.

[22] M. Haghifam and S. Fathi, "Distribution harmonic state estimation based on a hybrid PSO and SA algorithm considering parameters uncertainty," in *IEEE PES General Meeting (PESGM)*, Norway, Jul 2011.

[23] F. Ahmadi Gorjayi and H. Mohsenian-Rad, "Physics-aware sparse harmonic state estimation in power distribution systems," in *Proc. of the IEEE PES Conference on Innovative Smart Grid Technologies (ISGT), New Orleans, LA,*, Apr 2022.

[24] G. D'Antona, C. Muscas, and S. Sulis, "Localization of nonlinear loads in electric systems through harmonic source estimation," *IEEE Transactions on Instrumentation and Measurement*, vol. 60, no. 10, pp. 3423–3430, Oct 2011.

[25] R. Fernandes, M. Oleskovicz, and I. da Silva, "Harmonic source location and identification in radial distribution feeders: An approach based on particle swarm optimization algorithm," *IEEE Transactions on Industrial Informatics*, vol. 18, no. 5, pp. 3171–3179, May 2021.

[26] D. Carta, C. Muscas, P. Pegoraro, and S. Sulis, "Identification and estimation of harmonic sources based on compressive sensing," *IEEE Transactions on Instrumentation and Measurement*, vol. 68, no. 1, pp. 95–104, Jan 2019.

[27] X. Chen, W. Feng, C. Shuyu, S. Chew, and K. Tseng, "PMU placement for measurement redundancy distribution considering zero injection bus and contingencies," *IEEE Systems Journal*, vol. 14, no. 4, pp. 5396–5406, May 2020.

[28] X. Zhu, M. Wen, V. Li, and K. Leung, "Optimal PMU-communication link placement for smart grid wide-area measurement systems," *IEEE Transactions on Smart Grid*, vol. 10, no. 4, pp. 4446–4456, Jul 2018.

[29] Z. Zhihua, Z. Qu, and J. Yang, "Optimal harmonic measuring device placement in distribution networks in consideration of topology changes," *IEEE Access*, vol. 8, pp. 85 339–85 347, May 2020.

[30] W. Li, D. Deka, M. Chertkov, and M. Wang, "Real-time faulted line localization and PMU placement in power systems through convolutional neural networks," *IEEE Transactions on Power Systems*, vol. 34, no. 6, pp. 4640–4651, Nov2019.

[31] A. Akrami, S. Asif, and H. Mohsenian-Rad, "Sparse distribution system state estimation: An approximate solution against low observability," in *Proc. of the IEEE PES Conference on Innovative Smart Grid Technologies (ISGT)*, Feb 2020.

[32] A. Akrami, S.Asif, and H. Mohsenian-Rad, "Sparse tracking state estimation for low-observable power distribution systems using D-PMUs," *IEEE Transactions on Power Systems*, vol. 37, no. 1, pp. 551–564, Jan 2022.

[33] A. S. Zamzam and N. D. Sidiropoulos, "Physics-aware neural networks for distribution system state estimation," *IEEE Transactions on Power Systems*, vol. 35, no. 6, pp. 4347–4356, Nov 2020.

[34] M. Ghasemi Damavandi, V. Krishnamurthy, and J. Martí, "Robust meter placement for state estimation in active distribution systems," *IEEE Transactions on Smart Grid*, vol. 6, no. 4, pp. 1972–1982, Jul 2015.

[35] H. Mohsenian-Rad, *Smart Grid Sensors: Principles and Applications*. Cambridge University Press, UK, 2022.

[36] M. Farajollahi, A. Shahsavari, and H. Mohsenian-Rad, "Location identification of high impedance faults using synchronized harmonic phasors," in *IEEE PES ISGT, Arlington, VA,*, Apr 2017.

[37] M. Grant and S. Boyd, *CVX: Matlab software for disciplined convex programming, version 2.2,*. http://cvxr.com/cvx/, Jan, 2020.

[38] O. Wing, *Classical Circuit Theory*. Springer, New York, 2008.

[39] M. Farajollahi, A. Shahsavari, E. M. Stewart, and H. Mohsenian-Rad, "Locating the source of events in power distribution systems using micro-PMU data," *IEEE Transactions on Power Systems*, vol. 33, no. 6, pp. 6343–6354, May 2018.

[40] M. E. Baran and F. F. Wu, "Network reconfiguration in distribution systems for loss reduction and load balancing," *IEEE Transactions on Power Delivery*, vol. 4, no. 2, pp. 1401–1407, Apr 1994.

[41] R. Dugan, *Reference Guide: OpenDSS*. EPRI, July, 2010.

[42] *https://site.ieee.org/pes-testfeeders/resources*.

[43] N. V. Ramana, *Power System Analysis*. Pearson, 2010.

[44] D. Montenegro, R. Dugan, and G. Ramos, "Harmonics analysis using sequential-time simulation for addressing smart grid challenges," in *Proc. of 23rd Int. Conf. Electricity Distribution*, Lyon, France, Jun 2015.

Fatemeh Ahmadi-Gorjayi (S'20) received the B.Sc. degree in electrical engineering from Sharif University of Technology, Tehran, Iran, in 2013, and the M.Sc. degree in MBA, Operation Management and Supply Chain from the department of Industrial Engineering at University of Tehran, Tehran, Iran in 2018. She is currently pursuing her Ph.D. degree at the University of California, Riverside, CA, U.S. Her research interests include state estimation, power system harmonics, power system planning, and applications of data-driven techniques in power system.

Hamed Mohsenian-Rad (M'09-SM'14-F'20) received the Ph.D. degree in electrical and computer engineering from the University of British Columbia, Vancouver, BC, Canada, in 2008. He is currently a Professor of electrical engineering and a Bourns Family Faculty Fellow at the University of California, Riverside, CA, USA. His research is on monitoring, data analysis, and optimization of power systems and smart grids. He is the author of the textbook *Smart Grid Sensors: Principles and Applications* by Cambridge University Press - 2022. He was the recipient of the National Science Foundation (NSF) CAREER Award, the Best Paper Award from the IEEE Power & Energy Society General Meeting, the Best Paper Award from the IEEE Conference on Smart Grid Communications, and a Technical Achievement Award from the IEEE Communications Society. He has been the PI on ten million dollars research grants in the area of smart grid. He has served as Editor for the IEEE TRANSACTIONS ON POWER SYSTEMS, IEEE TRANSACTIONS ON SMART GRID and the IEEE POWER ENGINEERING LETTERS.